Influence of oxygen and water vapor on the structural transformations in nanogranular $(Co_{40}Fe_{40}B_{20})_x(LiNbO_3)_{100-x}$ composites

© A.V. Sitnikov [1,2], I.V. Babkina [1], Yu.E. Kalinin [1], A.E. Nikonov [1], M.N. Kopytin [1,¶], A.R. Shakurov [1], D.S. Pogrebnoi [1], V.V. Rylkov [2]

[1] Voronezh State Technical University,
Voronezh, Russia
[2] National Research Center „Kurchatov Institute“,
Moscow, Russia

¶ E-mail: michaelkopitin@mail.ru

Influence of oxygen and water vapor in vacuum chamber during the deposition process of $(Co_{40}Fe_{40}B_{20})_x(LiNbO_3)_{100-x}$ thin film nanocomposites on electrical properties has been investigated. A significant growth in the electrical resistivity of $(Co_{40}Fe_{40}B_{20})_x(LiNbO_3)_{100-x}$ nanocomposites has been established with an increase in reactive gases partial pressure (oxygen and water vapor). It has been found, that the recrystallization temperature of composites deposited in argon atmosphere also increases with metallic phase concentration. While the recrystallization temperature of $(Co_{40}Fe_{40}B_{20})_x(LiNbO_3)_{100-x}$ nanocomposites sinthesized in mixed atmosphere of Ar with the reactive gases (oxygen or water vapor) decreases due to increase of the heterogeneous structure oxidation.

Keywords: Metal-insulator nanocomposites, electrical resistivity, thermal stability, phase composition, oxygen, water vapor.

1. Introduction

Multicomponent heterogeneous systems with an amorphous structure have a unique combination of physical properties that are difficult to obtain in crystalline compounds [1–3]. Such materials can be used in devices for information storage [4], transparent electronics [5,6], different kinds of sensors [7,8] and other areas [9]. In particular, nanogranular composite $(Co_{40}Fe_{40}B_{20})_x(LiNbO_3)_{100-x}$ is a promising material for use as a functional environment in the development of memristive elements for creating multilevel memory and other devices that use the effect of reversible resistive switching (RS) from one state (high-resistance) to another (low-resistance) and back [10–12]. Optimization of the functional characteristics of memristors based on nanocomposites is associated with the possibility of purposeful change of the fine structure of the heterogeneous system and obtaining a material with predetermined properties. In previous papers it was found that oxygen vacancies in the dielectric phase [13,14] play a key role in the process of resistive switching in such systems. Another important factor responsible for the stability and multilevel character of RS is the concentration of embedded (dispersed) atoms of the metal phase in the dielectric matrix [11,12,15–18]. These factors are sensitive to the technology heterogeneous structures production, in particular, to the active gases (oxygen and water vapor) presence in the sputtering chamber.

Therefore, identification of their effect on the structure and electrical properties of the composite is an important task of obtaining functional environment with desired properties.

Since the amorphous state is thermodynamically unstable and can transform into a crystalline state upon heating, then the essential factor is the thermal stability of the electrical properties of the functional layer of the memristive element, which largely depends on the elementary composition and technological parameters of heterogeneous system synthesis. The physical properties of nanogranular composites and their thermal stability depend on the conditions of their synthesis and the presence of active gases in the sputtering chamber [19]. Such gases in the sputtering chamber can be oxygen atoms and water vapor. The latter can significantly affect the nature of the RS of memristors [20]. Taking into account the above said, the purpose of this paper was to establish the regularities of the effect of oxygen atoms and water vapor on the structure stability and phase composition of nanocomposites $(Co_{40}Fe_{40}B_{20})_x(LiNbO_3)_{100-x}$ under various thermal effects.

2. Experimental procedure

Thin films of nanocomposites $(Co_{40}Fe_{40}B_{20})_x(LiNbO_3)_{100-x}$ were obtained by method of ion-beam sputtering [19,21]. The sputtered target consisted

of a metal base of the $Co_{40}Fe_{40}B_{20}$ alloy with a size of $270 \times 80 \times 15$ mm, on the surface of which 16 plates of monocrystal compound $LiNbO_3$ with size $80 \times 10 \times 2$ mm were fixed unevenly along the length of the target. The nanocomposite was deposited simultaneously on five substrates 60×48 mm (or four, depending on the substrates orientation), which were located on the holder coaxially relative to the target at a distance of 200 mm from it in the form of a strip 240 mm long. This arrangement of the composite target and substrates made it possible, in one technological cycle, to obtain samples with different ratio of the dielectric and metallic phases in the range $x \approx 10-40$ at.% along the entire length of the strip. Glass-ceramic for electrical measurements and oxidized silicon for X-ray studies were used as substrates. The thickness of the nanocomposite films was $\sim 0.4 \mu m$. Three types of samples were prepared: without the active gases addition, with the addition of oxygen 1.8% and water vapor 3.2% in relation to argon.

The electrical resistance as function of temperature were measured in vacuum at a residual gas pressure of at least 10^{-5} Torr, and heating rate of $5°C$/min in the temperature range $20-600°C$. The samples were annealed in a vacuum at least 10^{-5} Torr at a fixed temperature for 30 min.

The structure of the obtained films was investigated by X-ray diffraction on a Bruker D2 Phaser diffractometer $(\lambda_{CuK_{\alpha1}} = 1.54$ Å) using the DIFFRAC.EVA 3.0 software and ICDD PDF database Release 2012.

3. Research results

3.1. Electric properties

The effect of oxygen atoms and water vapor on the concentration dependence of the electrical resistance of nanocomposites $(Co_{40}Fe_{40}B_{20})_x(LiNbO_3)_{100-x}$ is shown in Fig. 1. For composites obtained in Ar atmosphere, the electrical resistivity decreases from $\rho \approx 60 \Omega \cdot cm$ at $x = 11$ at.% of metal phase to $\rho \approx 0.01 \Omega \cdot cm$ at $x = 40$ at.%. The introduction of oxygen atoms or water vapor leads to increased electrical resistivity of the nanocomposites $(Co_{40}Fe_{40}B_{20})_x(LiNbO_3)_{100-x}$ in the entire studied concentrations range (curves *2* and *3*, respectively). In this case, the effect of oxygen atoms on the resistivity value is more significant than that of H_2O vapor, which is associated with increased oxidation state of the dielectric matrix and partial oxidation of the metal phase.

Electrical resistance $R(T)$ vs. temperature curves for nanocomposites $(Co_{40}Fe_{40}B_{20})_x(LiNbO_3)_{100-x}$ at the temperature rise from 20 to $600°C$ and then decreasing are shown in Fig. 2. During synthesis in Ar atmosphere the change of the electrical resistance of composites depends on the metallic phase concentration (Fig. 2, *a*): at a low concentration of the metallic phase (below the percolation threshold), the electrical resistance after recrystallization increases (curves *1−3*), and at high concentrations of
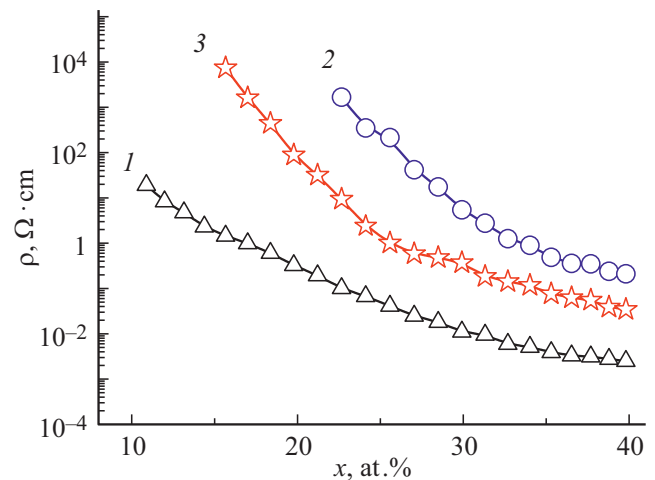
Figure 1. Electrical resistivity of composites $(Co_{40}Fe_{40}B_{20})_x(LiNbO_3)_{100-x}$, obtained in Ar atmosphere (curve *1*), upon addition of oxygen 1.8% (curve *2*) and water vapor 3.2% (curve *3*) vs. concentrations.

the metallic phase — decreases (curve *4*). In composite $(Co_{40}Be_{40}B_{20})_{36.5}(LiNbO_3)_{63.5}$ there is an area of a abrupt resistance decreasing at $\sim 500°C$ (curve *4*). Besides, in this sample a positive value of the temperature coefficient of resistance after cooling is observed, which is characteristic for metal films. This type of relationship allows to conclude that the studied compound is beyond the percolation threshold. In the case of nanocomposites $(Co_{40}Fe_{40}B_{20})_x(LiNbO_3)_{100-x}$ synthesized in an argon atmosphere both with the addition of 1.8% oxygen and 3.2% water vapor, the resistance increasing is observed for all compositions after recrystallization of the amorphous structure (Fig. 2, *b* and 2, *c*, respectively).

The characteristic feature of the samples obtained in an atmosphere of active gases is the observation of a maximum in the $R(T)$, which is most clearly manifested in the entire studied concentration range for nanocomposites grown in water vapor (Fig. 2, *c*). In the composite synthesized with the addition of oxygen $(Co_{40}Be_{40}B_{20})_{22.7}(LiNbO_3)_{73.3}$ at $\sim 380°C$ is weakly expressed due to the high value of the electrical resistance of this film. The general objective law of this feature manifestation in the $R(T)$ relationship is increased temperature of maximum observation upon increased concentration of the metal phase of the composite.

Note also that all samples synthesized in an atmosphere of active gases are characterized by increased electrical resistance after heat treatment in the temperature range $500-600°C$. During cooling the films under study, except for the case noted above, have a negative value of the temperature coefficient of electrical resistance, which is characteristic for semiconductors or „dirty" metals (for example, for amorphous films $Co_{40}Be_{40}B_{20}$; see Fig. 6 from [22]).
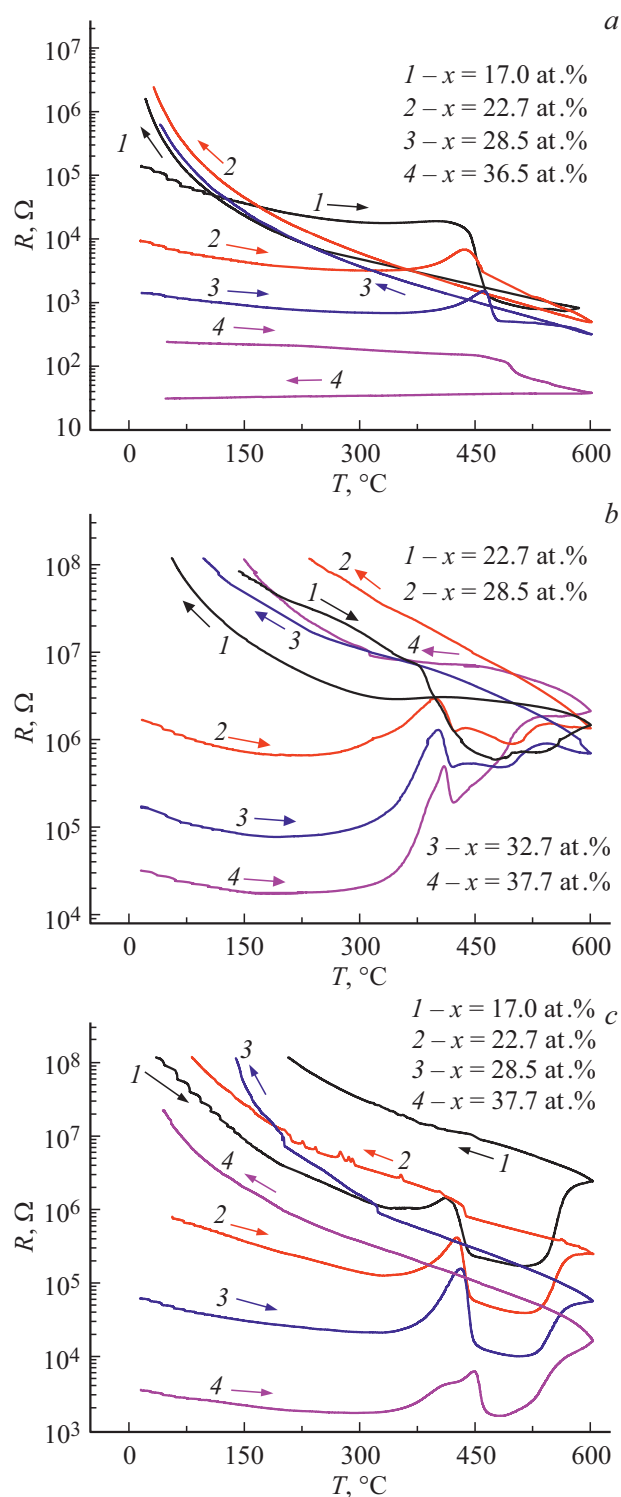
Figure 2. Electrical resistivity of composites $R(T)$ $(Co_{40}Fe_{40}B_{20})_x(LiNbO_3)_{100-x}$, obtained in Ar atmosphere (a), upon addition of oxygen 1.8% (b) and water vapor 3.2% (c) vs. temperature.

3.2. X-ray studies

To study changes in the phase composition of films during recrystallization, samples of nanocomposites

$(Co_{40}Fe_{40}B_{20})_x(LiNbO_3)_{100-x}$ were subjected to a series of heat treatments at temperatures from 300°C to 600°C through 50°C during 30°min in a vacuum chamber at residual gas pressure at least 10^{-5} Torr. Typical relationships of the X-ray reflection intensity $I(2\Theta)$ for films of nanocomposites $(Co_{40}Fe_{40}B_{20})_x(LiNbO_3)_{100-x}$, deposited in Ar atmosphere are shown in Fig. 3. It is seen that in the initial state and up to the annealing temperature of 400°C the films have an X-ray amorphous structure. After annealing at temperatures from 450−550°C a recrystallization process occurs, which exhibits in the appearance of maxima on the characteristic $I(2\Theta)$. After heat treatment at $T = 600$°C for 30°min the crystalline phase changes significantly with the formation of new chemical compounds. It should be noted that the formation of new compounds in the temperature range under study was observed only in composites obtained in an atmosphere of pure Ar with metal phase concentration of 17−28.5 at.% [23]. The diffraction patterns of all synthesized samples during the transition from the X-ray amorphous to the crystalline state had the same structure. The difference was observed only in the relative intensity of the revealed maxima. Therefore, Fig. 4, a shows the interpretation of the characteristic X-ray pattern for the nanocomposite $(Co_{40}Be_{40}B_{20})_{22.7}(LiNbO_3)_{77.3}$ synthesized in Ar atmosphere. Analysis of the obtained X-ray pattern showed that in the process of recrystallization two dielectric phases are formed: $LiNbO_3$ rhombohedral system and NbO_2 tetragonal system. During deposition and subsequent annealing the metallic phase is stabilized in the form of a granular CoFe alloy with a volume-centered cubic structure, as was previously identified from atomic resolution electron microscopy studies [11,24].
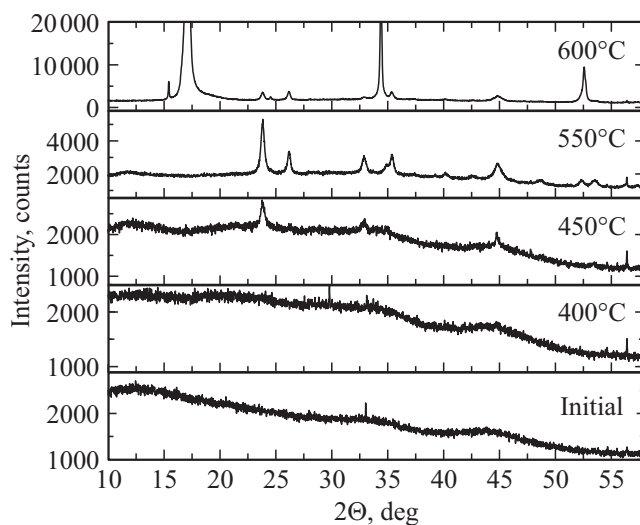
Figure 3. Diffraction patterns of film of nanocomposite $(Co_{40}Fe_{40}B_{20})_{22.7}(LiNbO_3)_{77.3}$, obtained in Ar atmosphere in initial state and after annealing in vacuum at different temperatures during time period 30 min.
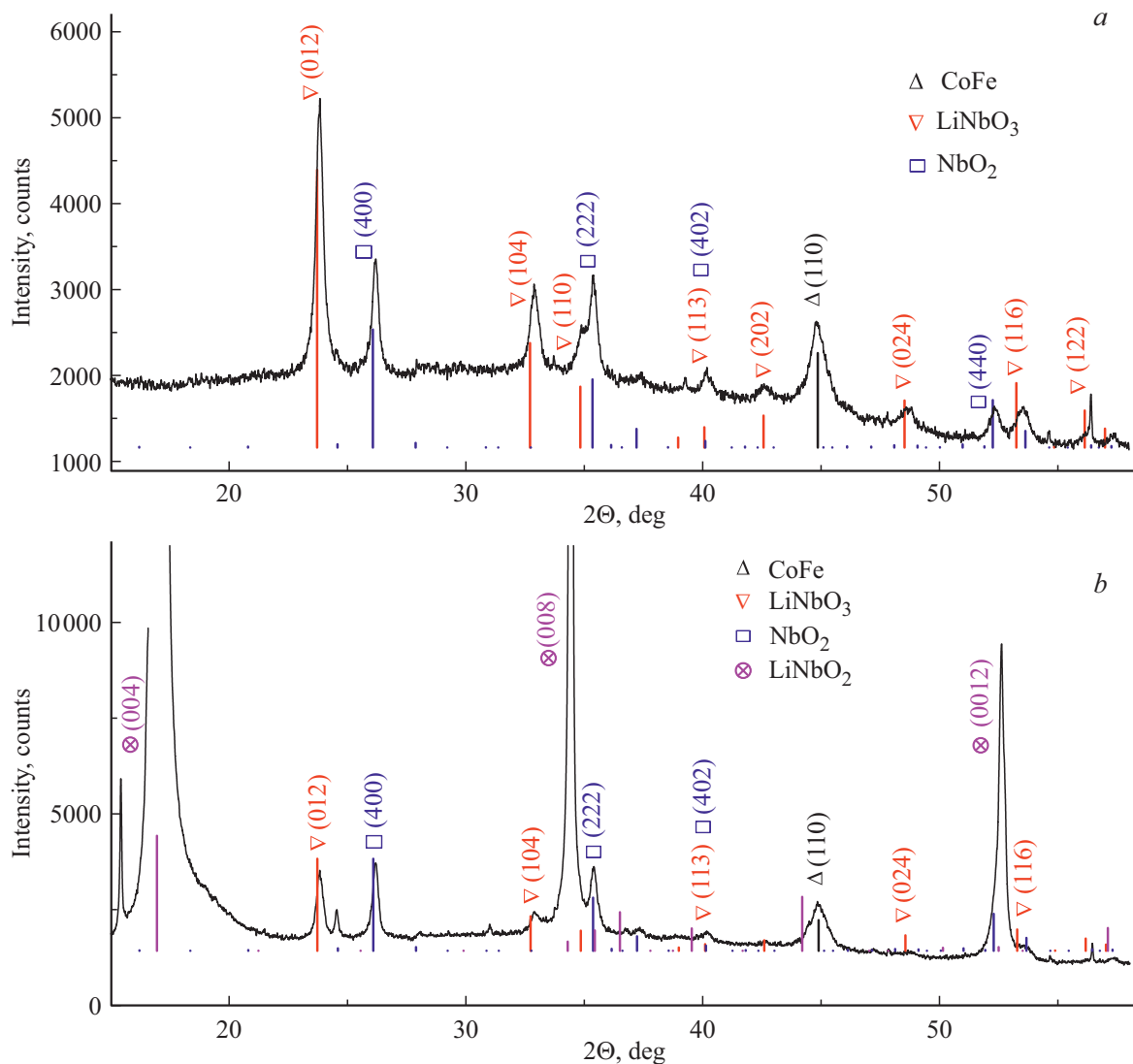
Figure 4. Diffraction patterns of film of nanocomposite $(Co_{40}Fe_{40}B_{20})_{22.7}(LiNbO_3)_{77.3}$, synthesized in an Ar atmosphere after heat treatment in vacuum during time period 30 min at 550°C (*a*) and at 600°C (*b*).

As noted above, at an annealing temperature $T = 600°C$ for 30 min in the samples obtained without adding active gases the crystalline phase changes significantly with the formation of new chemical compounds. Fig. 4, *b* shows interpretation of such diffractogram. In addition to the previously identified phases, maxima appear on the graph, they can be attributed to the compound $LiNbO_2$ of the hexagonal system. Note that the formed phase has a pronounced texture in the direction (004) to the film plane.

4. Discussion of obtained results

Our studies of the atomic structure of nanocomposites $(Co_{40}Fe_{40}B_{20})_x(LiNbO_3)_{100-x}$ ($x < 20$ at.%) by methods of high-resolution electron microscopy showed that the matrix $LiNbO_3$ is amorphous, and the CoFe nanogranules

have a crystalline volume-centered cubic structure with a lattice parameter of 0.285 nm and a size in the film plane $\sim 2-4$ nm [11,18]. The crystallinity of the granules indicates that significant part of boron during the nanocomposite growth appears in the oxide matrix, and its content in the granules is much less than 20 at.%, when the amorphization of the CoFeB alloy is significant during its synthesis in the form of thin films. These features lead to an interesting regularity: the recrystallization temperature determined from the maximum on the temperature dependence of the electrical resistance of nanocomposites (Fig. 2) obtained in Ar atmosphere increases with increasing of the metal phase content (curve *1* in Fig. 5).

The formation of nuclei of crystalline oxide phases $LiNbO_3$ and NbO_2 during annealing can be explained by a certain deficiency of Li atoms in the oxidized state in the amorphous insulating matrix. Besides, note that the relative amount of NbO_2 increases with increasing x at the

Comparison of enthalpies of formation and dissociation energies of Li and Nb of bonds with oxygen [21]

Reagents	Li		Nb	
	Enthalpy of formation ΔH_{f0}, kcal/mol	Bond-dissociation energy ΔH_0, kcal/mol	Enthalpy formation ΔH_{f0}, kcal/mol	Bond-dissociation energy ΔH_0, kcal/mol
O	15.7 ± 3	81 ± 3	48 ± 10	183 ± 10
O_2	-39.8 ± 1.5	93 ± 4	-50.1 ± 5	157 ± 10
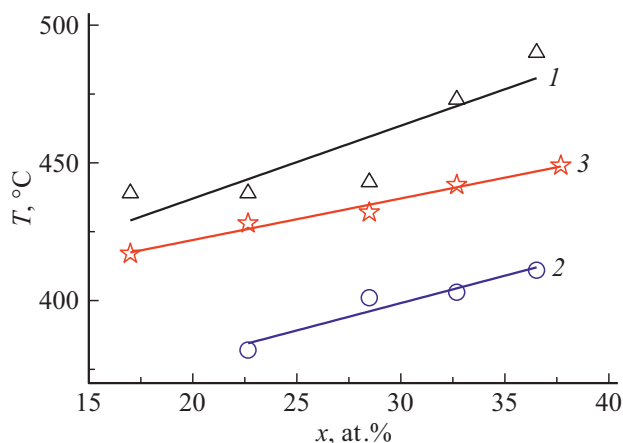
Figure 5. Concentration dependence of the maxima position of curves $R(T)$ associated with the recrystallization of nanocomposites $(Co_{40}Fe_{40}B_{20})_x(LiNbO_3)_{100-x}$, obtained in Ar atmosphere (curve *1*), by adding oxygen 1.8% (curve *2*) and water vapor 3.2% (curve *3*).

absence of active gases. The following mechanism for the occurrence of Li deficiency in the insulating matrix can be assumed. For this, we will consider the process of oxide synthesis during ion-plasma sputtering of the target. During impingement by argon ions of $LiNbO_3$ sub-samples both individual elements in the atomic state (Li, Nb and O), and in the form of compounds of various molecular compositions (LiO, NbO, LiNbO, etc.) can be knocked-out. The probability of formation of these sputtering products, which determines their relative concentration, depends on the bond energy between atoms. Based on this there should be more Li atoms in the flow of the sputtered compound $LiNbO_3$ than Nb because of the much lower bond dissociation energy of LiO as compared to NbO (see Table). As a result of surface diffusion of sputtering products, not only the nanostructured heterogeneous system $(Co_{40}Fe_{40}B_{20})_x(LiNbO_3)_{100-x}$ occurs, but also chemical reactions during the collision of active atoms and molecules. The probability of chemical reactions depends on the enthalpy of the given compound formation and the bond dissociation energy of the reaction product. From this point of view, Nb oxidation is more likely than Li oxidation. Due to the very limited lithium solubility in Co and Fe [25] and its low melting point 180°C, unoxidized Li atoms can be

thermally re-sputtered from the substrate surface and form metal nanogranules as a third phase in a heterogeneous system, or be dispersed in CoFe granules. The latter can explain the relative increasing of the amount of NbO_2 to $LiNbO_3$ with the concentration increasing of the metallic phase of the composite. With an active gases concentration increasing, the number of lithium atoms in the oxidized state, which are incorporated into the dielectric amorphous phase increases.

As it was mentioned above, in composites $(Co_{40}Fe_{40}B_{20})_x(LiNbO_3)_{100-x}$, obtained in Ar atmosphere, after annealing at temperature of 600°C for 30 min the crystalline oxide phase is noticeably modified due to the formation of a new compound $LiNbO_2$. This may be due to the significant nonstoichiometry of the dielectric phase of the system under consideration, as well as the interaction of metallic Li with compounds of the dielectric matrix. In this case, the chemical reaction $Li + NbO_2 = LiNbO_2$ is possible.

Let us now consider the possible reasons for the maximum occurrence in the temperature dependence of the resistance $R(T)$ at temperatures $T \sim T_c$, corresponding to the beginning of oxide recrystallization processes T_c (Fig. 2). It seems natural to associate the resistance increasing in the temperature range $T \leq T_c$, preceding the active phase of recrystallization, with the poor solubility of metals such as Fe(Co) in the oxide matrix of composites, and strong non-equilibrium of the arising heterogeneous system, in which the processes of the granules nucleation and their coalescences are temperature sensitive [18,19]. As a result of these processes, when the metal content is below the percolation threshold, the granules grow larger, the average distances between them increase, this leads to an resistance increasing of the nanocomposite [19]. This scenario is supported by the diffraction patterns of the samples subjected to heat treatment at temperatures below the recrystallization temperature of the dielectric phase (Fig. 6). It can be seen that the intensity maximum characterizing the nanocrystalline phase CoFe ($2\Theta \approx 45$ deg) begins to change significantly at $T \leq T_c$, which indicates a significant size increasing of nanocrystals of the metallic phase.

Meanwhile, the electrical resistance decreasing of nanocomposites at $T \geq T_c$, i.e. under conditions of oxide recrystallization, should apparently be associated with change in its electronic structure. Indeed, in the amorphous state
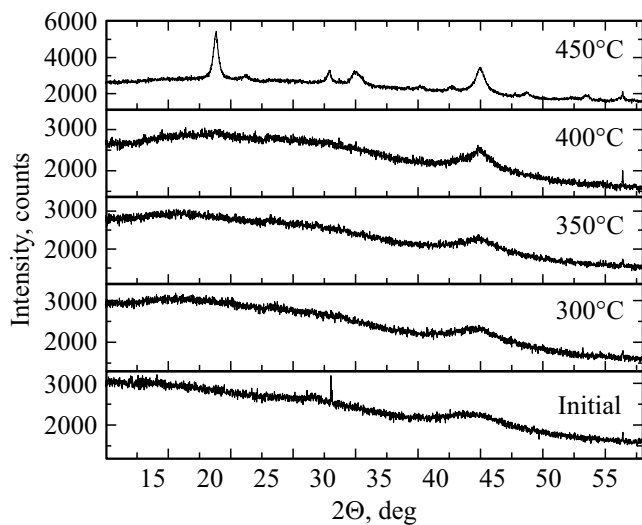
Figure 6. Diffraction patterns of film of nanocomposite $(Co_{40}Fe_{40}B_{20})_{28.5}(LiNbO_3)_{71.5}$, obtained in Ar atmosphere with the addition of water vapor 3.2% in initial state and after annealing in vacuum at different temperatures during time period 30 min.

of the dielectric its defects are determined by broken bonds, the energy levels of which extend deep into the forbidden zone of the material, pinning the Fermi level, which leads to increased effective intergranular barrier and decreased its tunneling conductivity. Meanwhile, in the crystalline state, the dominant defects of the oxide may be smaller defects such as oxygen vacancies [26], which will lead to a shift of the Fermi level to the boundaries of the conduction band or valence band and, accordingly, a decreased intergranular barrier and increased its tunneling conductivity.

With the recrystallization temperature T_c increasing at increased the concentration of the metal phase the another feature is closely related, namely, the recrystallization temperature decreasing when reactive gases are introduced into the sputtering chamber (Fig. 5). In this case, the oxygen introduction has a much greater effect on the recrystallization temperature (Fig. 5, curve *2*) as compared with the water vapor addition (Fig. 5, curve *3*). This behavior of T_c is explained by the fact that the active gases addition leads to increased oxidation state of the insulating matrix and partial oxidation of the metallic phase of the nanocomposite $(Co_{40}Fe_{40}B_{20})_x(LiNbO_3)_{100-x}$, as is confirmed by the significant difference in electrical resistivity of the samples under study (Fig. 1). With the reactive gases introduction the total concentration of the metal phase decreases, this is accompanied by decreased recrystallization temperature (Fig. 5).

Thus, the reactive gases introduction into the sputtering chamber during the ion-beam synthesis of nanocomposites $(Co_{40}Fe_{40}B_{20})_x(LiNbO_3)_{100-x}$ is accompanied by increased electrical resistivity of the synthesized films and decreased recrystallization temperature of composites as compared with films obtained in an argon atmosphere.

5.   Conclusion

The effect of oxygen molecules and water vapor introducing into the sputtering chamber during the synthesis of thin-film nanocomposites $(Co_{40}Fe_{40}B_{20})_x(LiNbO_3)_{100-x}$ on their electrical properties and structural transformations under thermal effects from 30 to 600°C. It is shown that recrystallization of the dielectric phase of the synthesized composites leads to the formation of compounds $LiNbO_3$ and NbO_2. In composites $(Co_{40}Fe_{40}B_{20})_x(LiNbO_3)_{100-x}$, obtained in atmosphere of pure argon during heat treatment at $T = 600°C$ for 30 min, the crystalline phase changes significantly due to the formation of additional compound $LiNbO_2$.

Increasing of the nanocomposites resistance $R(T)$ at temperatures lower than the oxide recrystallization temperature $T_c \sim 350-500°C$ is associated with increased size of metal nanogranules and intergranular gaps due to nucleation into granules dispersed in the matrix of Fe(Co) atoms, as well as coalescence of granules. Meanwhile, under the conditions of recrystallization of the dielectric phase of the heterogeneous system $(Co_{40}Fe_{40}B_{20})_x(LiNbO_3)_{100-x}$ the resistance increasing of nanocomposites is changed by its rather abrupt drop. The recrystallization temperature of the dielectric phase of nanocomposites $(Co_{40}Fe_{40}B_{20})_x(LiNbO_3)_{100-x}$, obtained in argon atmosphere, increases with concentration increasing of the metal phase, and decreases with oxidation state increasing of the heterogeneous structure by introducing the reactive gases — oxygen and water vapor into the sputtering chamber during the synthesis of films.

Work funding

Conflict of interest

The authors declare that they have no conflict of interest.

References

[1] L.E. Bykova, V.G. Myagkov, I.A. Tambasov, O.A. Bayukov, V.S. Zhigalov, K.P. Polyakova, G.N. Bondarenko, I.V. Nemtsev, V.V. Polyakov, G.S. Patrin, D.A. Velikanov. FTT **57**, *2*, 366 (2015). (in Russian)

[2] S.A. Gridnev, L.N. Korotkov. Amorphous materials based on perovskite ferroelectrics. Perovskites and other framework structure crystalline materials: new trends and perspectives — Collaborating Academics. P. 373. (2021).

[3] V.V. Rylkov, A.V. Emel'yanov, S.N. Nikolaev, K.E. Nikiruj, A.V. Sitnikov, E.A. Fadeev, V.A. Demin, A.B. Granovsky. ZhETF **158**, *1* (*7*), 164 (2020). (in Russian)

[4] D. Strukov, F. Alibart, R. Stanley Williams. Appl. Phys. A **107**, *4*, 509 (2012).

[5] O.V. Zhilova, S.Yu. Pankov, A.V. Sitnikov, Yu.E. Kalinin, M.A. Kashirin, V.A. Makagonov. Mater. Res. Express **6**, *8*, 086330 (2019).

[6] M.N. Volochaev, A.B. Granovsky, O.V. Zhilova, Yu.E. Kalinin, V.V. Ryl'kov, M.P. Sumets, V.A. Makagonov, S.Yu. Pankov, A.V. Sitnikov, E. Fadeev, E. Lahderanta, V.A. Foshin. Superlat. Microstruct. **140**, 106449 (2020).

[7] A.A. Bukharaev, A.K. Zvezdin, A.P. Pyatakov, Yu.K. Fetisov. UFN **188**, *12*, 1288 (2018). (in Russian)

[8] K. Toshio, H. Hideo. NPG Asia Mater. **2**, *1*, 15 (2010).

[9] S. Sanctis, J. Krausmann, C. Guhl, J.J. Schneider. J. Mater. Chem. C **6**, *3*, 464 (2018).

[10] V.V. Ryl'kov, A.B. Drovosekov, A.N. Taldenkov, S.N. Nikolaev, O.G. Udalov, A.V. Emel'yanov, A.V. Sitnikov, K.Yu. Chernoglazov, V.A. Demin, O.A. Novodvorsky, A.S. Vedeneev, A.S. Bugaev. ZhETF **155**, *1*, 127 (2019). (in Russian)

[11] V.V. Ryl'kov, S.N. Nikolaev, V.A. Demin, A.V. Emel'yanov, A.V. Sitnikov, K.E. Nikiruj, V.A. Levanov, M.Yu. Presnyakov, A.N. Taldenkov, A.L. Vasiliev, K.Yu. Chernoglazov, A.S. Vedeneev, Yu.E. Kalinin, A.B. Granovsky, V.V. Tugushev, A.S. Bugaev. ZhETF **153**, *3*, 424 (2018). (in Russian)

[12] V.V. Ryl'kov, A.V. Emel'yanov, S.N. Nikolaev, K.E. Nikiruj, A.V. Sitnikov, E.A. Fadeev, V.A. Demin, A.B. Granovsky. ZhETF **158**, *1* (*7*), 164 (2020). (in Russian)

[13] E.V. Okulich, V.I. Okulich, D.I. Tetelbaum. Pis'ma v ZhTF **46**, *1*, 24 (2020). (in Russian)

[14] S.N. Nikolaev, A.V. Emel'yanov, R.G. Chumakov, V.V. Ryl'kov, A.V. Sitnikov, M.Yu. Presnyakov, E.V. Kukueva, V.A. Demin. ZhTF **90**, *2*, 257 (2020). (in Russian)

[15] I.V. Bykov, E.A. Gan'shina, A.B. Granovsky, V.S. Gushchin. FTT **42**, *3*, 487 (2000). (in Russian)

[16] V. Rylkov, A. Sitnikov, S. Nikolaev, A. Emelyanov, K. Chernohlazov, K. Nikiruy, A. Drovosekov, M. Blinov, E. Fadeev, A. Taldenkov, V. Demin, A. Vedeneev, A. Bugaev, A. Granovsky. IEEE Magn. Lett. **10**, 2509504 (2019).

[17] A.V. Sitnikov, I.V. Babkina, Yu.E. Kalinin, A.E. Nikonov, M.N. Kopytin, K.E. Nikiruj, A.I. Il'yasov, K.Yu. Chernoglazov, S.N. Nikolaev, A.L. Vasiliev, A.V. Emel'yanov, V.A. Demin, V.V. Ryl'kov. Nanoindustriya **13**, *S5-3* (*102*), 687 (2020). (in Russian)

[18] M.N. Martyshov, A.V. Emelyanov, V.A. Demin, K.E. Nikiruy, A.A. Minnekhanov, S.N. Nikolaev, A.N. Taldenkov, A.V. Ovcharov, M.Yu. Presnyakov, A.V. Sitnikov, A.L. Vasiliev, P.A. Forsh, A.B. Granovsky, P.K. Kashkarov, M.V. Kovalchuk, V.V. Rylkov. Phys. Rev. Appl. **14**, *3*, 034016 (2020).

[19] S.A. Gridnev, Yu.E. Kalinin, A.V. Sitnikov, O.V. Stognej. Nelinejnye yavleniya v nano- i mikrogeterogennykh sistemakh. Binom. Laboratoriya znanij, M. (2012). 352 p. (in Russian)

[20] I. Valov, T. Tsuruoka. J. Phys. D **51**, *41*, 413001 (2018).

[21] V.V. Rylkov, V.A. Demin, A.V. Emelyanov, A.V. Sitnikov, Yu.E. Kalinin, V.V. Tugushev, A.B. Granovsky. Novel Magnetic Nanostructures: Unique Properties and Applications / Ed. N. Domracheva, M. Caporali, E. Rentschler, Elsevier (2018). P. 427.

[22] G.V. Swamy, P.K. Rout, M. Singh, R.K. Rakshit. J. Phys. D **48**, 475002 (2015).

[23] A.V. Sitnikov, I.V. Babkina, Yu.E. Kalinin, A.E. Nikonov, M.N. Kopytin, A.R. Shakurov, V.V. Ryl'kov. ZhTF **91**, *9*, 1393 (2021). (in Russian)

[24] V.V. Rylkov, S.N. Nikolaev, K.Yu. Chernoglazov, V.A. Demin, A.V. Sitnikov, M.Yu. Presnyakov, A.L. Vasiliev, N.S. Perov, A.S. Vedeneev, Yu.E. Kalinin, V.V. Tugushev, A.B. Granovsky. Phys. Rev. B **95**, 144202 (2017).

[25] N.P. Lyakishev, O.A. Bannykh, L.L. Rokhlin et al. Spravochnik: Diagrammy sostoyaniya dvojnykh metallicheskikh sistem. Spravochnik. Mashinostoenie, M. (1997). V. 2. 1024 p. (in Russian)

[26] T.V. Perevalov. Electronnaya struktura vakansij kisloroda v oksidakh alyuminiya, gafniya, tantala i titana. Avtoref. kand. dis. Novosibirsk (2015). 22 p. (in Russian)